# Stable three-dimensional spinning optical solitons supported by competing quadratic and cubic nonlinearities

February 3, 2008

D. Mihalache[1], D. Mazilu[1], L.-C. Crasovan[1], I. Towers[2], B. A. Malomed[2], A. V. Buryak[3], L. Torner[4], and F. Lederer[5]

[1]Department of Theoretical Physics, Institute of Atomic Physics, PO Box MG-6, Bucharest, Romania
[2]Faculty of Engineering, Tel Aviv University, Tel Aviv 69978, Israel
[3]School of Mathematics and Statistics, University of New South Wales at ADFA, Canberra, ACT 2600, Australia
[4]Department of Signal Theory and Communications, Universitat Politecnica de Catalunya, ES 08034 Barcelona, Spain
[5]Institute of Solid State Theory and Theoretical Optics, Friedrich-Schiller University Jena, Max-Wien-Platz 1, D-07743, Jena, Germany

## Abstract

We show that the quadratic interaction of fundamental and second harmonics in a bulk dispersive medium, combined with self-defocusing cubic nonlinearity, give rise to completely localized spatiotemporal solitons (vortex tori) with vorticity $s = 1$. There is no threshold necessary for the existence of these solitons. They are found to be stable if their energy exceeds a certain critical value, so that the stability domain occupies about 10 % of the existence region of the solitons. On the contrary to spatial vortex solitons in the same model, the spatiotemporal ones with $s = 2$ are never stable. These results might open the way for experimental observation of spinning three-dimensional solitons in optical media.

# 1 Introduction

Solitons, i.e., self-trapped light beams or pulses that are supported by a balance between diffraction and/or dispersion and nonlinearity, are prominent objects in nonlinear optics [1]. Optical spatiotemporal solitons (STS) [2], alias superspikes [3] or light bullets [4], were predicted in many works [2] - [16]. They result from the simultaneous balance of diffraction and group-velocity dispersion (GVD) by self-focusing. Although they cannot be stable in the uniform self-focusing Kerr ($\chi^{(3)}$) medium [8], stability can be achieved in saturable [3, 6, 10], quadratically nonlinear ($\chi^{(2)}$) [2, 12, 13, 14], and graded-index Kerr media [15]. STS can also be found in off-resonance two-level systems [17], in self-induced-transparency media [18], as well as in engineered tandem structures incorporating quadratically nonlinear slices [19].

While a fully localized "light bullet" in three dimensions (3D) has not yet been found in an experiment, two-dimensional (2D) STS in a bulk $\chi^{(2)}$ medium were observed in Ref. [20]. That work reported the formation of pulses in quadratic media, which overcome diffraction in one transverse spatial dimension and GVD in the longitudinal direction. However, such experiments were performed by means of the tilted-pulse technique, which employs highly elliptical beams; therefore, diffraction is negligible in the remaining transverse spatial dimension.

Optical vortex solitons constitute another class of self-supporting objects, that have attracted much attention because of possible applications to the all-optical processing of information, or to guiding and trapping of atoms. The concepts of a multidimensional optical soliton and of an optical vortex may be combined, giving rise to *spinning* (vortex) solitons. Starting with the seminal works [21], both delocalized ("dark") and localized ("bright") optical vortices were investigated in various 2D environments [22, 23, 24, 25]. In the 3D case, the bright spinning solitons take the shape of a torus ("doughnut") [26, 27].

For bright vortex solitons, stability is a major concern, as, unlike their zero-spin counterparts, the spinning solitons are apt to be destabilized by azimuthal perturbations. For 2D models with $\chi^{(2)}$ nonlinearities, an azimuthal instability was discovered by simulations [28] and observed experimentally [29]. As a result, a soliton with spin 1 splits into three or two fragments in the form of separating zero-spin soliton. Numerical simulations of the 3D spinning STS in the $\chi^{(2)}$ model also demonstrates splitting into moving zero-spin solitons [27].

Nevertheless, the $\chi^{(2)}$ nonlinearity acting in combination with the self-*defocusing* Kerr [$\chi^{(3)}_{-}$, where we use the subscript "minus" to stress the self-repulsion] nonlinearity gives rise to stable spinning (ring-shaped) 2D solitons with spin $s = 1$ and 2 [23]. Models of this type for spatial [(2+1)-dimensional] solitons are well known [30, 31]. The stability of the spinning solitons in the $\chi^{(2)} : \chi^{(3)}_{-}$ model may be realized as a result of competition between the self-focusing and self-defocusing nonlinearities. This understanding is further supported by the fact

that stable spinning solitons of the same type have also been found in another optical model displaying both focusing and defocusing nonlinearities, viz., the one based on the cubic-quintic (CQ) nonlinear Schrödinger (NLS) equation. In addition to optics, the same equations have been investigated in the contexts of Bose-Einstein condensates (BECs) [32] and Langmuir waves in plasmas [33] (however, in the former case, the quintic nonlinearity arises from three-body interactions, which also give rise to losses by recombination of BEC constituents into different species, thus making the quintic nonlinear coefficient a complex one).

In the first direct simulations of 2D solitons with spin 1 in the CQ model, reported in the pioneer work [34], it was found that they are robust, provided that their energy is not too small [34]. Later analysis, based on the computation of linear-stability eigenvalues, demonstrated that some of the spinning 2D solitons considered in Ref. [34] are subject to a weak azimuthal instability. Nonetheless, in another part of their existence region, where they have a very large energy, the solitons with spin $s = 1$ and $s = 2$ were confirmed to be stable in the 2D CQ model [35] (see also Ref. [36] for the stability investigation of the solitons with spin $s = 1$). Stable 2D vortex solitons in the CQ model can self-trap from Gaussian inputs with an embedded vorticity [37]. Notice that all the solitons with $s \geq 3$ have been demonstrated to be unstable in the CQ model [35].

A challenging issue is the search for physically relevant models in which *stable* 3D spinning solitons exist. In fact, the only previously known model which could support stable 3D vortex solitons was the Skyrme model (see reviews [38]). Very recently, we have found stable 3D spinning STS in the CQ model, which could again be construed as a result of the competition between self-focusing and self-defocusing [39]. Direct simulations of the 3D CQ model [40] demonstrated that 3D spinning solitons with moderate energies were unstable against azimuthal perturbations, while the ones with very large energies, i.e., broad "doughnuts" with a small hole in the center, were robust under propagation. However, a consistent stability analysis makes it necessary to compute eigenvalues of small perturbations. By calculating the instability growth rates, in Ref. [39] it was rigorously shown that sufficiently broad STS with spin $s = 1$ are stable, the stability region occupying $\approx 20\%$ of their existence region, while all the STS with $s \geq 2$ are unstable.

The aim of this paper is to show that the existence of stable spinning 3D solitons is a more generic fact, which is not limited to the CQ model considered in Ref. [39]. To this end, we will analyze the existence and stability of spinning STS solitons in the 3D version of the above-mentioned $\chi^{(2)} : \chi_{-}^{(3)}$ model with the self-defocusing cubic term. In section 2, the model is formulated, and general results concerning the existence of 3D spinning STS in it, with different values of the spin, are displayed. Fundamental results for the stability of the spinning solitons, based on eigenvalues found from equations linearized around the soliton solutions, are presented in section 3. Direct simulations of the solitons' stability

within the framework of the full nonlinear equations are displayed in section 4, and section 5 concludes the work.

## 2 The model and spinning solitons

The scaled equations describing the reversible generation of the second harmonic (SH) from a single fundamental-frequency (FF) component $u$, in the presence of the self-defocusing cubic nonlinearity, dispersion and diffraction in the (3+1)-dimensional geometry, are well known [12, 13, 23, 30, 31]:

$$
\begin{aligned}
&i\frac{\partial u}{\partial Z}+\frac{1}{2}\left(\frac{\partial^2 u}{\partial X^2}+\frac{\partial^2 u}{\partial Y^2}+\frac{\partial^2 u}{\partial T^2}\right)+u^*\,v\,-(|u|^2+2|v|^2)u\,=0,\\
&i\frac{\partial v}{\partial Z}+\frac{1}{4}\left(\frac{\partial^2 v}{\partial X^2}+\frac{\partial^2 v}{\partial Y^2}+\sigma\frac{\partial^2 v}{\partial T^2}\right)-\beta v+u^2\,-2(2|u|^2+|v|^2)v\,=0. \qquad (1)
\end{aligned}
$$

Here, $T$, $X$, $Y$ and $Z$ are the normalized reduced time, transverse spatial coordinates, and propagation distance, $u$ and $v$ are envelopes of the FF and SH fields, and $\beta$ is a phase mismatch between the FF and SH waves. In particular, the variables used in Eqs. (1) are related to their counterparts (to be denoted by tildes) in Ref. [23] as follows: $u \equiv 2\widetilde{u}$, $v \equiv \widetilde{w}$, $\sqrt{2}\,(x,y) \equiv (\widetilde{x},\widetilde{y})$.

Equations (1) assume different GVD coefficients at the two harmonics, $\sigma$ being their ratio [12], but neglects the Poynting-vector walkoff between the harmonics, and assumes that the temporal group-velocity mismatch between them [14, 41, 42] has been compensated. On the other hand, in the case $\sigma = 1$ the model possesses an additional spatiotemporal spherical symmetry [12, 13]. Below, we will display results for the case $\sigma = 1$, assuming that the group-velocity mismatch may be neglected in this case too.

We look for stationary solutions to Eqs. (1) in the form $u = U(r,T)\exp\left(i\kappa Z + is\theta\right)$, $v = V(r,T)\exp\left[2\left(i\kappa Z + is\theta\right)\right]$, where $\theta$ is the polar angle in the plane $(x,y)$, $\kappa$ is a wave number shift, and the integer $s$ is the above-mentioned spin. The amplitudes $U$ and $V$ may be taken real, obeying the equations

$$
\begin{aligned}
&\frac{1}{2}\left(\frac{\partial^2 U}{\partial r^2}+\frac{1}{r}\frac{\partial U}{\partial r}-\frac{s^2}{r^2}U+\frac{\partial^2 U}{\partial T^2}\right)-\kappa U+UV-(U^2+2V^2)U=0,\\
&\frac{1}{4}\left(\frac{\partial^2 V}{\partial r^2}+\frac{1}{r}\frac{\partial V}{\partial r}-\frac{4s^2}{r^2}V+\sigma\frac{\partial^2 V}{\partial T^2}\right)-(2\kappa+\beta)V+U^2-2(2U^2+V^2)V=0. \qquad (2)
\end{aligned}
$$

Dynamical equations (1) conserve the total energy

$$
E \;=\; \int\int\int (|u|^2+|v|^2)dXdYdT \equiv E_u + E_v, \qquad (3)
$$

Hamiltonian

$$
H \;=\; \frac{1}{2}\int\int\int\left\{\left[(|u_X|^2+|u_Y|^2+|u_T|^2)+\frac{1}{4}(|v_X|^2+|v_Y|^2+\sigma|v_T|^2)\right]\right.
$$

$$+\left[\beta|v|^2-(u^{*2}v+u^2v^*)+(|u|^4+4|u|^2|v|^2+|v|^4)\right]\Bigg\}dXdYdT\,, \quad (4)$$

momentum (equal to zero for the solutions considered), and longitudinal component of the orbital angular momentum $L$ [43]. The following relations between $L$, $H$ and $E$ for a stationary spinning STS follow from Eqs. (2): $L = sE$, and

$$H=-\frac{1}{3}\kappa E+\frac{1}{3}\beta E_v-\frac{1}{3}\int\int\int\left(|u|^4+4|u|^2|v|^2+|v|^4\right)dXdYdT. \quad (5)$$

We have numerically found one-parameter families of stationary 3D spinning solitons which have the shape of a doughnut with a hole (supported by a phase dislocation) in the center. To this end, we solved numerically the coupled system of equations (2) using a standard band-matrix algorithm [44] to deal with the corresponding two-point boundary-value problem. We will display results for $\sigma = 1$; however, we have also found that the STS exist for all $\sigma \geq 0$, cf. Ref. [13], where nonspinning STS were studied in detail for $\sigma \neq 1$.

In Fig. 1 we summarize the output of extensive numerical calculations aimed to detect the domains of existence and stability of spinning STS. The continuous lines border the existence domain, and the dashed line constitutes a boundary between stable and unstable regions in the parameter plane $(\beta, \kappa)$. The way the stability boundary has been found will be explained in detail in the following sections.

Shapes of three representative doughnut-like *stable* STS are plotted in Fig. 2 for a fixed value of the net energy [see Eq. (3)], $E = 12000$. We see that, with the increase of the mismatch $\beta$, the energy of the FF component of the spinning soliton increases, similar to the case of nonspinning solitons in pure $\chi^{(2)}$ media [42, 45, 46, 47].

Below, we present systematic results which characterize spinning STS in the case of the zero phase matching, $\beta = 0$. In Fig. 3 we plot the curves $\kappa = \kappa(E)$ and $H = H(E)$ for *both* nonspinning and spinning STS in this case. The full and dashed lines in Fig. 3 correspond to stable and unstable branches according to results presented below. The $s = 0$ solitons are stable according to the known Vakhitov-Kolokolov (VK) criterion, which states that the fundamental ($s = 0$) soliton branch undergoes a stability change at the point $dE/d\kappa = 0$ [48].

A feature shared by the nonspinning and spinning solitons, as it is evident in Fig. 3, is the absence of any finite threshold for their existence. This is a drastic difference from the recently studied STS in the CQ model, where well-defined thresholds were found for zero and nonzero values of the spin [26, 39].

# 3 Stability eigenvalues of the spinning solitons

Complete understanding of the stability of solitons is provided by direct simulations of the evolution equations (see below) together with the analysis of Eqs.

(1) linearized about the stationary spinning-soliton solution. In this section, we focus on the latter approach, seeking for perturbation eigenmodes in a general form,

$$\begin{aligned} & u(Z,r,T,\theta) - U(r,T)\exp\left[i(s\theta+\kappa Z)\right] \\ = \; & f(r,T)\exp\left\{\lambda_n Z + i[(s+n)\theta+\kappa Z]\right\} + g^*(r,T)\exp\left\{\lambda_n^* Z + i[(s-n)\theta+\kappa Z]\right\}, \quad (6) \\ & v(Z,r,T,\theta) - V(r,T)\exp\left[2i(s\theta+\kappa Z)\right] \\ = \; & p(r,T)\exp\left\{\lambda_n Z + i[(2s+n)\theta+2\kappa Z]\right\} + q^*(r,T)\exp\left\{\lambda_n^* Z + i[(2s-n)\theta+2\kappa Z]\right\}, \quad (7) \end{aligned}$$

where $n > 0$ is an arbitrary integer azimuthal index of the perturbation, $\lambda_n$ is the (complex) eigenvalue that needs to be found, and functions $f$, $g$ and $p$, $q$ obey equations

$$\begin{aligned} i\lambda_n f + \frac{1}{2}\left[\frac{\partial^2 f}{\partial T^2} + \frac{\partial^2 f}{\partial r^2} + r^{-1}\frac{\partial f}{\partial r} - (s+n)^2 r^{-2} f\right] - \kappa f & \\ -2\left(U^2+V^2\right) f - \left(U^2 - V\right) g - (2UV - U)\, p - 2UVq &= 0, \quad (8) \\ -i\lambda_n g + \frac{1}{2}\left[\frac{\partial^2 g}{\partial T^2} + \frac{\partial^2 g}{\partial r^2} + r^{-1}\frac{\partial g}{\partial r} - (s-n)^2 r^{-2} g\right] - \kappa g & \\ -2\left(U^2+V^2\right) g - \left(U^2 - V\right) f - (2UV - U)\, q - 2UVp &= 0, \quad (9) \\ i\lambda_n p + \frac{1}{4}\left[\sigma\frac{\partial^2 p}{\partial T^2} + \frac{\partial^2 p}{\partial r^2} + r^{-1}\frac{\partial p}{\partial r} - (2s+n)^2 r^{-2} p\right] - (2\kappa+\beta)p & \\ -4\left(U^2+V^2\right) p - 2V^2 q - 2\,(2UV - U)\, f - 4UVg &= 0, \quad (10) \\ -i\lambda_n q + \frac{1}{4}\left[\sigma\frac{\partial^2 q}{\partial T^2} + \frac{\partial^2 q}{\partial r^2} + r^{-1}\frac{\partial q}{\partial r} - (2s-n)^2 r^{-2} q\right] - (2\kappa+\beta)q & \\ -4\left(U^2+V^2\right) q - 2V^2 p - 2\,(2UV - U)\, g - 4UVf &= 0, \quad (11) \end{aligned}$$

Physical solutions must decay exponentially at $r \to \infty$. At $r \to 0$, $f$ and $g$ must vanish as $r^{|s\pm n|}$, whereas $p$ and $q$ vanish as $r^{|2s\pm n|}$.

To solve the above equations and find the eigenvalues, we used a known numerical procedure [28, 49], which produces results presented in Fig. 4. The most persistent unstable eigenmode is found for value of the azimuthal index $n = 2$, for both $s = 1$ and $s = 2$. As is seen in Fig. 4, the instability of the soliton with $s = 1$, accounted for by $\mathrm{Re}\,\lambda_2$, disappears with the increase of $\kappa$ at a stability-change point, $\kappa_{\rm st} \approx 0.04572$, and the stability region extends up to $\kappa = \kappa_{\rm offset}^{(3D)} \approx 0.051$, corresponding to the upper continuous line in Fig. 1, i.e., infinitely broad solitons (which implies that the vortex of the dark-soliton type [21], that may be regarded as an infinitely broad spinning soliton, is stable too). The relative width of the stability region is $\left(\kappa_{\rm offset}^{(3D)} - \kappa_{\rm st}\right)/\kappa_{\rm offset}^{(3D)} \approx 0.1$. However, *no* stability region has been found for the 3D solitons with $s = 2$, as well as in the 3D model of the CQ type, and in contrast to the 2D vortex solitons in both the $\chi^{(2)} : \chi_{-}^{(3)}$ model with the competing quadratic and cubic nonlinearities (the same as considered here) [23], and 2D CQ model [35].

In the case when the spinning solitons are unstable, their instability is *oscillatory*; the corresponding frequency, Im$\lambda$ [see Figs. 4 (c) and 4(d)] is found to be, generally, on the same order of magnitude as Re$\lambda$ at the maximum-instability point. In the stable region, $\kappa \geq \kappa_{\rm st}$, all the eigenvalues are purely imaginary. Oscillatory instabilities of solitons, characterized by complex eigenvalues of the corresponding non-self-adjoint linear operator, are typical to other conservative models of nonlinear optics [50, 51, 52].

# 4 Direct simulations

The above results were checked against direct simulations of Eqs. (1), carried out by means of the Crank-Nicholson scheme. The corresponding system of nonlinear partial differential equations was solved by means of the Picard iteration method [53], and the resulting linear system was handled by means of the Gauss-Seidel iterative scheme. For good convergence we needed, typically, five Picard iterations and fifteen Gauss-Seidel iterations. We employed a transverse grid having $121 \times 121 \times 91$ points, and a typical longitudinal step size was $\Delta Z = 0.1$. To avoid distortion of the instability development under the action of the periodicity imposed by the Cartesian computational mesh, we added initial perturbations that were mimicking random fluctuations in a real system (cf. Ref. [10]).

To illustrate the evolution of a stable 3D "bullet" generated by an input in the form of a completely localized Gaussian pulse with the energy $E_0 = 5986$ [see Eq. (3)], into which a vortex with $s = 1$ was embedded, in Fig. 5 we show the energies of its two components vs. $Z$. Robustness of the spinning STS is attested to by the fact that it can be generated from a Gaussian with a nested vortex, whose shape is far from the soliton's exact form. We see from Fig. 5 that there is a strong reshaping of the input Gaussian, which leads to a redistribution of the energy between the two components; some energy loss occurs, caused by emission of radiation in the course of the formation of the stable STS. Figure 6 shows gray-scale contour plots of the intensity and phase distribution in the FF component, in both the input Gaussian with a nested vortex, and in the emerging spinning STS with the vorticity $s = 1$ at $Z = 100$, corresponding to the same case which was presented in Fig. 5. No further essential evolution of the soliton was observed in this case at $Z > 100$.

Typical instabilities of the spinning STS with the spin $s = 1$ (in the case when it is unstable) and $s = 2$ are illustrated by Figs. 7 through 10. The azimuthal instability breaks the unstable spinning solitons into zero-spin ones, which fly out tangentially relative to the circular crest of the original soliton [similar to what is known about the instability-induced breakup of the (2+1)D spatial vortex solitons [28]]. Thus, the initial internal angular momentum (spin) of the doughnut-shaped spinning soliton is converted into the orbital momentum of the emerging nonspinning fragments.

Analyzing a large body of numerical results, we have concluded that the number of the emerging fragments is roughly equal to twice the original spin $s$. The dependence of the number of the fragments on the other parameters is fairly weak.

It is noteworthy that, in all the cases displayed in Figs. 7 through 10 (and in many more cases not shown here), the number of the instability-generated fragments is exactly equal to the azimuthal index of the perturbation mode having the largest growth rate. Thus, the full nonlinear evolution of the unstable spinning solitons is in perfect agreement with the stability analysis based on the linearized equations, which was presented in the previous section.

# 5 Conclusion

In this paper, we have shown that stable bright spatiotemporal spinning solitons (vortex tori), which were recently found in the cubic-quintic model of a dispersive optical medium with competing self-focusing and defocusing nonlinearities [39], are also possible in a model based on the competition between the quadratic and self-defocusing cubic nonlinearities. The solitons are stable, provided that they are broad enough (so that the soliton's energy exceeds a certain critical value, or, in other words, the size of the internal hole is essentially smaller than the overall size of the soliton).

In fact, the model with the $\chi^{(2)} : \chi_{-}^{(3)}$ (quadratic-cubic) nonlinearity may be realized easier in real optical media than the $\chi_{+}^{(3)} : \chi_{-}^{(5)}$ (self-focusing-cubic – self-defocusing-quintic) one. Possibilities for the experimental implementation of the former model (chiefly, based on the quasi-phase-matching technique) were discussed in Refs. [23, 54, 55]. Note that such optical media may be used equally well for the experimental generation of both the spatial (2+1)-dimensional solitons (vortex cylinders) considered in Ref. [23] and the 3D spatio-temporal spinning solitons (vortex tori) found in the present work.

It is relevant to stress that the amplitude of a beam that can give rise to a stable spinning soliton should not be specifically large: as it is evident from Fig. 2, the necessary power is essentially the same as that which is necessary for the existence of a nonspinning soliton. The difference from the latter case is that the beam generating a stable spinning soliton must be broad (its cross section and temporal width should be large), i.e., its peculiarity is not a large power but rather large total energy.

Similar to the cubic-quintic model, only spatiotemporal solitons with spin $s = 1$ may be stable in the present system, in contrast with the spatial (2+1)-dimensional solitons, which may be stable in the cases $s = 1$ and $s = 2$, in models of both types (on the other hand, a difference from the cubic-quintic case is that the existence of STS in the present model is not limited by any energy threshold). These results suggest a conclusion that stable vortex solitons are generic objects, provided that the medium's nonlinearity contains competing elements and the

soliton's energy is large enough; in all the known models lacking the nonlinear competition, bright vortex solitons are subject to a strong azimuthal instability.

Lastly, one can assume that, very generally speaking, the spinning soliton is not an absolutely stable object, but rather a metastable one. Indeed, the energy of the spinning soliton is larger than that of its zero-spin counterpart, hence it might be possible that a very strong initial perturbation will provoke its rearrangement into a zero-spin soliton, the angular moment being carried away with emitted radiation. In terms of this consideration, it appears that the $s = 1$ and $s = 0$ solitons are separated by extremely high potential barriers, which make the assumed process practically impossible. To illustrate this point, in Fig. 11 we show the cross sections of the $s = 1$ soliton which was very strongly perturbed at the initial point, $Z = 0$ (the perturbation is $\approx 30\%$ of the soliton's amplitude), and the result of its evolution at the point $Z = 200$. For the same case, the comparison of the distributions of the intensity and phase inside the initial strongly perturbed soliton and the finally established one are shown in Fig. 12 (cf. Fig. 6). As is obvious from Figs. 11 and 12, the soliton was able to completely heal the damage, remaining a truly stable object.

## acknowledgments

D. Mihalache, D. Mazilu and L.-C. Crasovan acknowledge support from the Deutsche Forschungsgemeinschaft (DFG) and European Community (Access to Research Infrastructure Action of the Improving Human Potential Program). I.T. and B.A.M. appreciate support from the Binational (US-Israel) Science Foundation through the grant No. 1999459, and a matching support from the Tel Aviv University. L.T. acknowledges support by TIC2000-1010.

## References


[1] G. I. Stegeman, D. N. Christodoulides, and M. Segev, IEEE J. Select. Top. Quant. Electron. **6**, 1419 (2000).

[2] A. A. Kanashov and A. M. Rubenchik, Physica D **4**, 122 (1981).

[3] J. T. Manassah, P. L. Baldeck, and R. R. Alfano, Opt. Lett. **13**, 1090 (1988); J. T. Manassah, *ibid.* **16**, 563 (1991).

[4] Y. Silberberg, Opt. Lett. **15**, 1282 (1990).

[5] A. B. Blagoeva *et al.*, IEEE J. Quant. Electr. **QE-27**, 2060 (1991).

[6] N. Akhmediev and J. M. Soto-Crespo, Phys. Rev. A **47**, 1358 (1993).

[7] Y. Chen and J. Atai, Opt. Lett. **20**, 133 (1995).

[8] L. Bergé, Phys. Rep. **303**, 260 (1998).

[9] R. H. Enns *et al.*, Opt. Quant. Electron. **24**, S1295 (1992); R. McLeod, K. Wagner, and S. Blair, Phys. Rev. A **52**, 3254 (1995); J. T. Manassah and B. Gross, Laser Phys. **7**, 9 (1997).

[10] D. E. Edmundson, Phys. Rev. E **55**, 7636 (1997).

[11] V. Skarka, V. I. Berezhiani, and R. Miklaszewski, Phys. Rev. E **56**, 1080 (1997).

[12] K. Hayata and M. Koshiba, Phys. Rev. Lett. **71**, 3275 (1993); B. A. Malomed *et al.*, Phys. Rev. E **56**, 4725 (1997); D. V. Skryabin and W. J. Firth, Opt. Commun. **148**, 79 (1998); D. Mihalache, D. Mazilu, B. A. Malomed, and L. Torner, *ibid.* **152**, 365 (1998).

[13] D. Mihalache, D. Mazilu, J. Dörring, and L. Torner, Opt. Commun. **159**, 129 (1999).

[14] D. Mihalache, D. Mazilu, B. A. Malomed, and L. Torner, Opt. Commun. **169**, 341 (1999); D. Mihalache, D. Mazilu, L.-C. Crasovan, L. Torner, B. A. Malomed, and F. Lederer, Phys. Rev. E **62**, 7340 (2000).

[15] S. Raghavan and G. P. Agrawal, Opt. Commun. **180**, 377 (2000).

[16] H. E. Nistazakis, D. J. Frantzeskakis, and B. A. Malomed, Phys. Rev. E **64**, 026604 (2001); C. Polymilis, D. J. Frantzeskakis, A. N. Yannacopoulos, K. Hizanidis, and G. Rowlands, J. OPt. Soc. Am. B **18** , 75 (2001).

[17] I. V. Mel'nikov, D. Mihalache, and N.-C. Panoiu, Opt. Commun. **181**, 345 (2000).

[18] M. Blaauboer, B. A. Malomed, and G. Kurizki, Phys. Rev. Lett. **84**, 1906 (2000).

[19] L. Torner, S. Carrasco, J. P. Torres, L.-C. Crasovan, and D. Mihalache, Opt. Commun. **199**, 277 (2001).

[20] X. Liu, L. J. Qian, and F. W. Wise, Phys. Rev. Lett. **82**, 4631 (1999); X. Liu, K. Beckwitt, and F. Wise, Phys. Rev. E **62**, 1328 (2000).

[21] G. A. Swartzlander, Jr., and C. T. Law, Phys. Rev. Lett. **69**, 2503 (1992); A. W. Snyder, L. Poladian, and D. J. Mitchell, Opt. Lett. **17**, 789 (1992).

[22] P. Di Trapani *et al.*, Phys. Rev. Lett. **84**, 3843 (2000).

[23] I. Towers, A.V. Buryak, R.A. Sammut, and B.A. Malomed, Phys. Rev. E **63**, 055601(R) (2001).

[24] A. S. Desyatnikov and Yu. S. Kivshar, Phys. Rev. Lett. **87**, 033901 (2001).

[25] Z. H. Musslimani, M. Soljacic, M. Segev, and D. N. Christodoulides, Phys. Rev. E **63**, 066608 (2001).

[26] A. Desyatnikov, A. Maimistov, and B. Malomed, Phys. Rev. E **61**, 3107 (2000).

[27] D. Mihalache, D. Mazilu, L.-C. Crasovan, B. A. Malomed, and F. Lederer, Phys. Rev. E **62**, R1505 (2000).

[28] L. Torner and D. V. Petrov, Electr. Lett. **33**, 608 (1997); W. J. Firth and D. V. Skryabin, Phys. Rev. Lett. **79**, 2450 (1997); J. P. Torres, J. M. Soto-Crespo, L. Torner, and D. V. Petrov, J. Opt. Soc. Am. B **15**, 625 (1998); D. V. Skryabin and W. J. Firth, Phys. Rev. E **58**, 3916 (1998).

[29] D. V. Petrov *et al.*, Opt. Lett. **23**, 1444 (1998).

[30] A. V. Buryak, Yu. S. Kivshar, and S. Trillo, Opt. Lett. **20**, 1961 (1995), M. A. Karpierz, Opt. Lett. **20**, 1677 (1995).

[31] O. Bang, J. Opt. Soc. Am. B **14**, 51 (1997); O. Bang, Yu. S. Kivshar, and A. V. Buryak, Opt. Lett. **22**, 1680 (1997); L. Berge, O. Bang, J. Juul Rasmussen, and V. K. Mezentsev, Phys. Rev. E **55**, 555 (1997); O. Bang, Yu. S. Kivshar, A. V. Buryak, A. De Rossi, and S. Trillo, Phys. Rev. E **58**, 5057 (1998).

[32] F. Kh. Abdullaev, A. Gammal, L. Tomio, and T. Frederico, Phys. Rev. A **63**, 043604 (2001); A. Gammal, T. Frederico, L. Tomio, and F. Kh. Abdullaev, Phys. Lett. A **267**, 305 (2001).

[33] C. T. Zhou and X. T. He, Physica Scripta, **50**, 415 (1994).

[34] M. Quiroga-Teixeiro and H. Michinel, J. Opt. Soc. Am. B **14**, 2004 (1997).

[35] I. Towers *et al.*, Phys. Lett. A **288**, 292 (2001); B. A. Malomed, L.-C. Crasovan, D. Mihalache, Physica D **161**, 187 (2002); R. L. Pego and H. A. Warchall, Los Alamos e-print archive: nlin.PS/0108009.

[36] V. I. Berezhiani, V. Skarka, and N. B. Aleksic, Phys. Rev. E **64**, 057601 (2001).

[37] H. Michinel *et al.* J. Opt. B: Quantum Semiclass. Opt. **3**, 314 (2001).

[38] D. O. Riska, Adv. Nucl. Phys. **22**, 1 (1996); T. Gisiger and M. B. Paranjape, Phys. Rep. **306**, 110 (1998).

[39] D. Mihalache, D. Mazilu, L.-C. Crasovan, I. Towers, A. V. Buryak, B. A. Malomed, L. Torner, J. P. Torres, and F. Lederer, Phys. Rev. Lett. **88**, 073902 (2002).

[40] D. Mihalache, D. Mazilu, L.-C. Crasovan, B. A. Malomed, and F. Lederer, Phys. Rev. E **61**, 7142 (2000).

[41] L. Torner, D. Mazilu, and D. Mihalache, Phys. Rev. Lett. **77**, 2455 (1996); C. Etrich, U. Peschel, F. Lederer, and B. A. Malomed, Phys. Rev. E **55**, 6155 (1997).

[42] C. Etrich, F. Lederer, B. A. Malomed, T. Peschel, and U. Peschel, Progress in Optics **41**, 483 (2000).

[43] N. N. Akhmediev and A. Ankiewicz, *Solitons, Nonlinear Pulses and Beams* (Chapman and Hall, London, 1997).

[44] G. Dahlquist and Å. Björk, *Numerical Methods*, (Prentice Hall, Englewood Cliffs, 1974).

[45] G. I. Stegeman, D. J. Hagan, and L. Torner, Opt. Quantum Electron. **28**, 1691 (1996).

[46] L. Torner and A. P. Sukhorukov, Opt. Photonics News **13**, 26 (2002).

[47] Yu. S. Kivshar, in *Advanced Photonics with Second-Order Optically Nonlinear Processes*, edited by A. D. Boardman, L. Pavlov, and S. Panev (Kluwer Academic, Dordrecht,1998), p. 451.

[48] M. G. Vakhitov and A.A. Kolokolov, Radiophys. Quantum El. **16**, 783 (1973).

[49] J. M. Soto-Crespo, D. R. Heatley, E. M. Wright, and N. N. Akhmediev, Phys. Rev. A **44**, 636 (1991); J. Atai, Y. Chen, and J. M. Soto-Crespo, Phys. Rev. A **49**, R3170 (1994).

[50] N. N. Akhmediev, A. Ankiewicz, and H. T. Tran, J. Opt. Soc. Am. B **10**, 230 (1993).

[51] B. A. Malomed and R. S. Tasgal, Phys. Rev. E **49**, 5787 (1994); I. V. Barashenkov, D. E. Pelinovsky, and E. V. Zemlyanaya, Phys. Rev. Lett. **80**, 5117 (1998); A. De Rossi, C. Conti, and S. Trillo, Phys. Rev. Lett. **81**, 85 (1998); J. Schöllmann, R. Scheibenzuber, A. S. Kovalev, A. P. Mayer, and A. A. Maradudin, Phys. Rev. E **59**, 4618 (1999).

[52] D. Mihalache, D. Mazilu, and L. Torner, Phys. Rev. Lett. **81**, 4353 (1998); D. Mihalache, D. Mazilu, and L.-C. Crasovan, Phys. Rev. E **60**, 7504 (1999).

[53] J. M. Ortega, W. C. Rheinboldt, *Iterative Solution of Nonlinear Equations in Several Variables*, (Academic Press, New York, 1970), p. 182.

[54] J. F. Corney and O. Bang, Phys. Rev. E **64**, 047601 (2001).

[55] S. K. Johansen, S. Carrasco, L. Torner, O. Bang, Opt. Commun. **203**, 393 (2002).

# Figure Captions

Fig. 1. Domains of the existence and stability of spinning STS with spin $s = 1$. The upper continuous curve is the existence border, corresponding to infinitely broad (in fact, dark) solitons.

Fig. 2. Typical shapes of stable STS with $s = 1$ for $E = 12000$: (a) $\beta = -0.1$, (b) $\beta = 0$, and (c) $\beta = 0.2$. The labels FF and SH pertain to the fundamental-frequency and second-harmonic components of the soliton.

Fig. 3. The propagation constant $\kappa$ (a) and Hamiltonian $H$ (b) of the three-dimensional solitons, with different values of spin, vs. their energy $E$, in the case of zero phase mismatch, $\beta = 0$.

Fig. 4. The growth rate of perturbations, Re $\lambda$, corresponding to different values of the azimuthal index $n$ (indicated by labels near the curves) vs. the soliton's wave number $\kappa$: (a) $s = 1$; (b) $s = 2$. The imaginary part of the stability eigenvalue, Im $\lambda$, corresponding to different values of the azimuthal index $n$ (indicated by labels near the curves) vs. the soliton's wave number $\kappa$: (c) $s = 1$; (d) $s = 2$. Here and in the following plots, $\beta = 0$. We stress that, in the case $s = 1$, the instability growth rate vanishes at the point $\kappa = \kappa_{\rm st}$, see the text, while in the case $s = 2$ the growth rate corresponding to $n = 2$ remains positive up to the border of the existence region of the solitons. This border is marked in all the panels by vertical arrows.

Fig. 5. Evolution of the energy components $E_u$ and $E_v$ of the soliton with $s = 1$, as generated by an input configuration in the form of a Gaussian with a nested vortex. Here, the input total energy is $E = 5986$.

Fig. 6. The formation of the soliton with spin $s = 1$ in the same case which corresponds to Fig. 5, shown in terms of the cross section of the fields at $T = 0$: (a) the intensity distribution in the initial Gaussian with a nested vortex; (b) its phase field; (c) the intensity distribution of the spinning soliton at $Z = 100$; (d) the phase field at $Z = 100$.

Fig. 7. Isosurface plots illustrating the fragmentation of the $s = 1$ soliton with $\kappa = 0.01$ into zero-spin ones as a result of the azimuthal instability: (a) $Z = 0$; (b) $Z = 1000$.

Fig. 8. The same as in Fig. 7 in the case $\kappa = 0.032$: (a) $Z = 0$; (b) $Z = 1140$.

Fig. 9. The same as in Figs. 7 and 8 in the case of the $s = 2$ initial soliton with $\kappa = 0.015$: (a) $Z = 0$; (b) $Z = 900$.

Fig. 10. The same as in Fig. 9 in the case $\kappa = 0.04$: (a) $Z = 0$; (b) $Z = 2100$.

Fig. 11. Cross sections of an $s = 1$ soliton that was strongly perturbed at $Z = 0$, and the result of its evolution after having passed the propagation distance $Z = 200$.

Fig. 12. The recovery of the soliton with spin $s = 1$ in the same case as in Fig. 11, shown in terms of the cross section of the fields at $T = 0$ (cf. Fig. 6): (a) the intensity distribution in the initial strongly perturbed soliton; (b) its

phase field; (c) the intensity distribution of the self-cleared soliton at $Z = 100$; (d) the phase field at $Z = 100$.

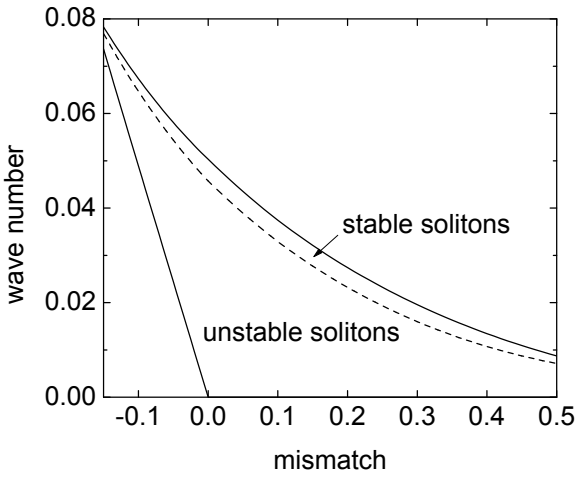
0.08
0.06
0.04
0.02
0.00
wave number
stable solitons
unstable solitons
-0.1
0.0
0.1
0.2
0.3
0.4
0.5
mismatch

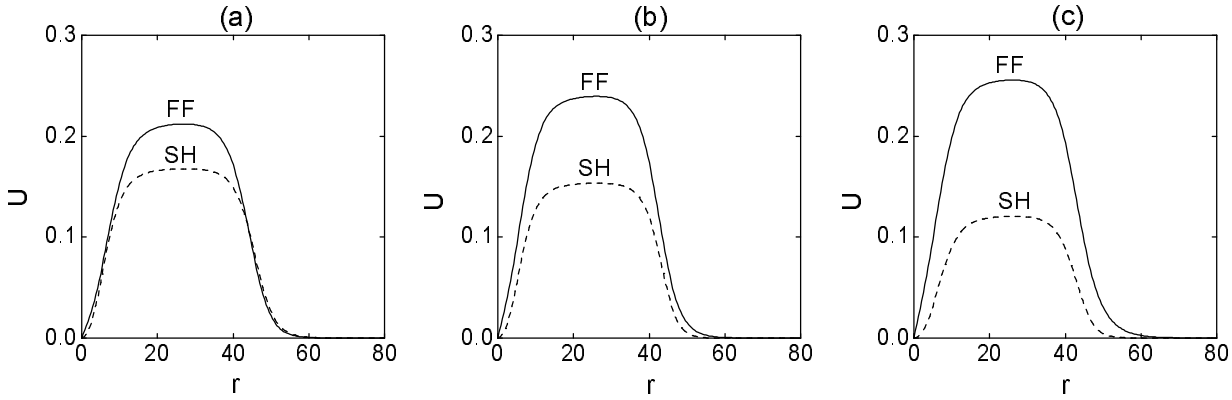
(a)
(b)
(c)
FF
SH
U
r
0.0
0.1
0.2
0.3
0
20
40
60
80

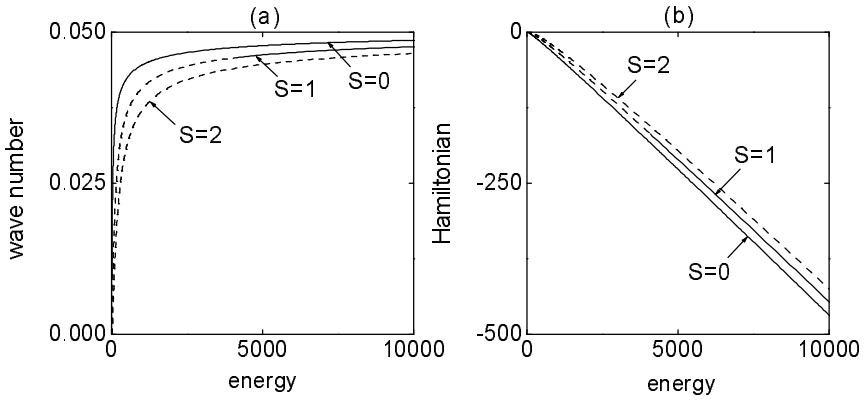
(a)
0.050
0.025
0.000
wave number
0
5000
10000
energy
S=0
S=1
S=2
(b)
0
-250
-500
Hamiltonian
0
5000
10000
energy
S=2
S=1
S=0

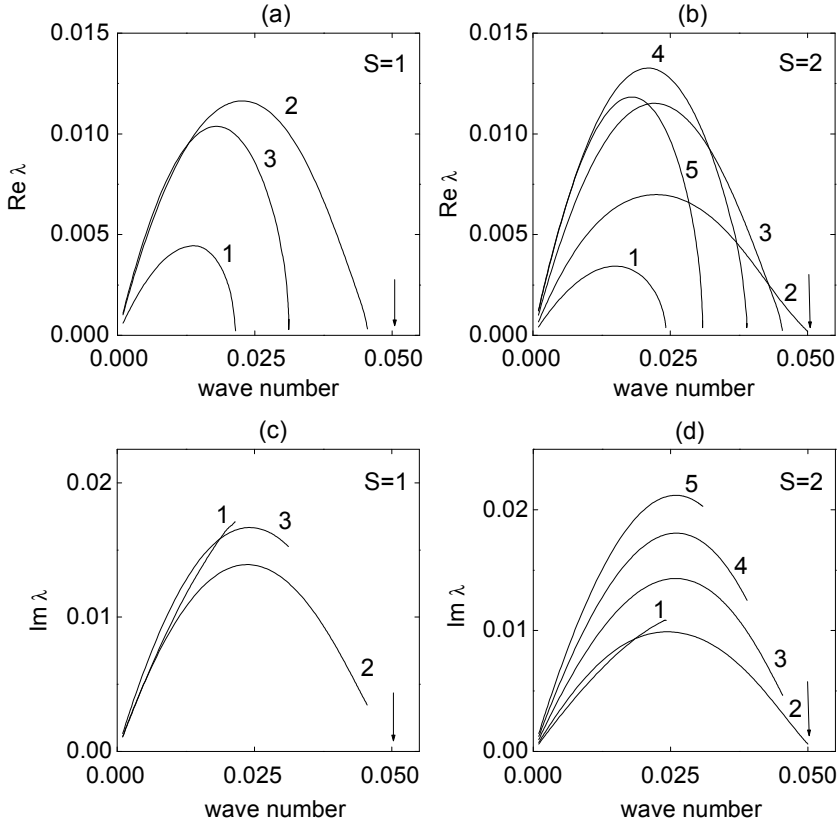
(a)
S=1
Re λ
0.015
0.010
0.005
0.000
0.000
0.025
0.050
wave number
1
2
3
(b)
S=2
Re λ
0.015
0.010
0.005
0.000
0.000
0.025
0.050
wave number
1
2
3
4
5
(c)
S=1
Im λ
0.02
0.01
0.00
0.000
0.025
0.050
wave number
1
2
3
(d)
S=2
Im λ
0.02
0.01
0.00
0.000
0.025
0.050
wave number
1
2
3
4
5

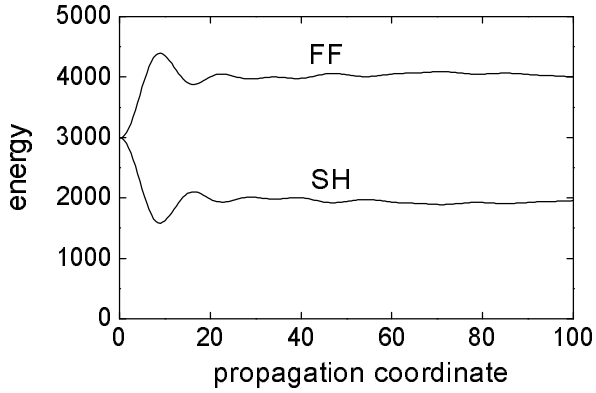
5000
4000
3000
2000
1000
0
energy
FF
SH
0
20
40
60
80
100
propagation coordinate

This figure "Fig6.jpg" is available in "jpg"  format from:

http://arXiv.org/ps/nlin/0206007v1

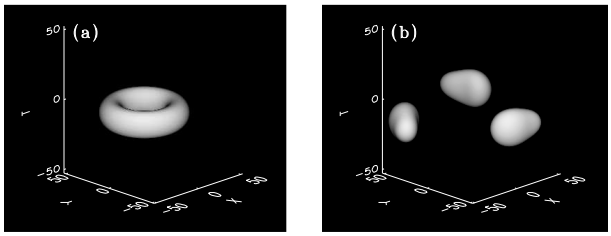
(a)
50
0
-50
Y
-50
0
50
X
-50
0
50
Z
(b)
50
0
-50
Y
-50
0
50
X
-50
0
50
Z

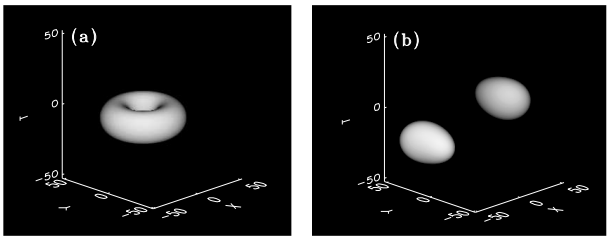
(a)
50
0
−50
z
−50
0
50
y
−50
0
50
x
(b)
50
0
−50
z
−50
0
50
y
−50
0
50
x

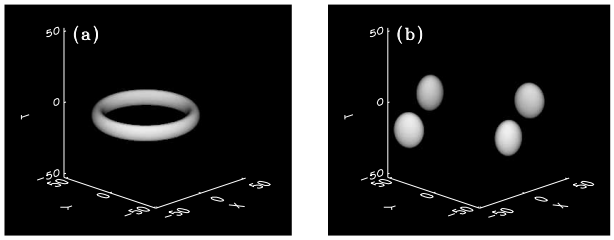
(a)
50
0
−50
z
−50
0
50
x
−50
0
50
y
(b)
50
0
−50
z
−50
0
50
x
−50
0
50
y

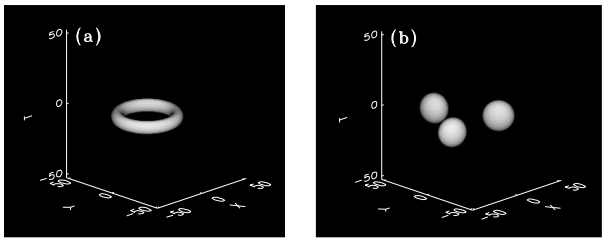
(a)
50
0
−50
Z
−50
0
Y
−50
0
X
50
(b)
50
0
−50
Z
−50
0
Y
−50
0
X
50

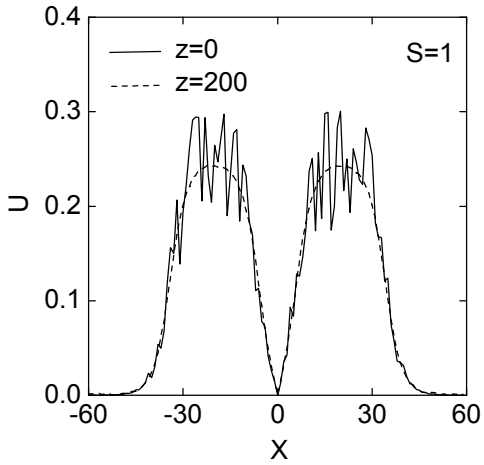
0.4
0.3
0.2
0.1
0.0
U
-60
-30
0
30
60
X
z=0
z=200
S=1

This figure "Fig12.jpg" is available in "jpg"  format from:

http://arXiv.org/ps/nlin/0206007v1